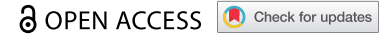


RESEARCH PAPER



## MIR106A-5p upregulation suppresses autophagy and accelerates malignant phenotype in nasopharyngeal carcinoma

Qingwen Zhu<sup>a,b</sup>, Qicheng Zhang<sup>a,b</sup>, Miao Gu<sup>a,b</sup>, Kaiwen Zhang<sup>a,b</sup>, Tian Xia<sup>a,b</sup>, Siyu Zhang<sup>a,b</sup>, Wenhui Chen<sup>a,b</sup>, Haimeng Yin<sup>a,b</sup>, Hui Yao<sup>a,b</sup>, Yue Fan<sup>a,b</sup>, Si Pan<sup>a,b</sup>, Haijing Xie<sup>a,b</sup>, Huiting Liu<sup>a,b</sup>, Tianyi Cheng<sup>a,b</sup>, Panpan Zhang<sup>a,b</sup>, Ting Zhang<sup>a,b</sup>, Bo You<sup>a,b</sup>, and Yiwen You<sup>a,b</sup>

<sup>a</sup>Department of Otorhinolaryngology Head and Neck Surgery, Affiliated Hospital of Nantong University, Nantong, Jiangsu Province, China; <sup>b</sup>Institute of Otolaryngology Head and Neck Surgery, Affiliated Hospital of Nantong University, Nantong, Jiangsu Province, China

### ABSTRACT

Dysregulated microRNAs (miRNAs) are involved in carcinoma progression, metastasis, and poor prognosis. We demonstrated that in nasopharyngeal carcinoma (NPC), transactivated *MIR106A-5p* promotes a malignant phenotype by functioning as a macroautophagy/autophagy suppressor by targeting *BTG3* (BTG anti-proliferation factor 3) and activating autophagy-regulating MAPK signaling. *MIR106A-5p* expression was markedly increased in NPC cases based on quantitative real-time PCR, miRNA microarray, and TCGA database analysis findings. Moreover, *MIR106A-5p* was correlated with advanced stage, recurrence, and poor clinical outcomes in NPC patients. In addition to three-dimensional cell culture assays, zebrafish and BALB/c mouse tumor models revealed that overexpressed *MIR106A-5p* targeted *BTG3* and accelerated the NPC malignant phenotype by inhibiting autophagy. *BTG3* promoted autophagy, and its expression was correlated with poor prognosis in NPC. Attenuation of autophagy, mediated by the *MIR106A-5p*-*BTG3* axis, occurred because of MAPK pathway activation. *MIR106A-5p* overexpression in NPC was due to increased transactivation by EGR1 and SOX9. Our findings may lead to novel insights into the pathogenesis of NPC.

**Abbreviations:** ACTB: actin beta; ATG: autophagy-related; ATG5: autophagy related 5; BLI: bioluminescence; BTG3: BTG anti-proliferation factor 3; CASP3: caspase 3; ChIP: chromatin immunoprecipitation; CQ: chloroquine; Ct: threshold cycle; DAPI: 4',6-diamidino-2-phenylindole; DiL: 1,1'-dioctadecyl-3,3,3',3'-tetramethylindocarbocyanine perchlorate; EBSS: Earle's balanced salt solution; EGR1: early growth response 1; GAPDH: glyceraldehyde-3-phosphate dehydrogenase; GEO: Gene Expression Omnibus; GFP: green fluorescent protein; IF: immunofluorescence; IHC: immunohistochemistry; ISH: *in situ* hybridization; MAP1LC3B: microtubule associated protein 1 light chain 3 beta; MIR106A-5p: microRNA 106a-5p; miRNAs: microRNAs; MKI67: marker of proliferation ki-67; mRNA: messenger RNA; MTOR: mechanistic target of rapamycin kinase; NPC: nasopharyngeal carcinoma; qRT-PCR: quantitative real-time PCR; siRNA: small interfering RNA; SOX9: SRY-box transcription factor 9; SQSTM1: sequestosome 1; TCGA: The Cancer Genome Atlas; WB: western blot.

### ARTICLE HISTORY

Received 22 August 2019  
Revised 28 May 2020  
Accepted 1 June 2020

### KEYWORDS

Autophagy; BTG3; malignant phenotype; *MIR106A-5p*; nasopharyngeal carcinoma




## Introduction

Nasopharyngeal carcinoma (NPC) is the most common form of head and neck cancer and is particularly prevalent in southern China and regions of Southeast Asia [1]. Recurrence and distant metastases are key indicators for aggressive and life-threatening NPC. Therefore, identification of molecular mechanisms associated with malignant NPC, including markers for development and metastasis, is crucial.


microRNAs (miRNAs) encompass a cluster of small non-coding RNAs that are post-transcriptional negative regulators of mRNA that act by binding to the 3'-untranslated region (3'-UTR) of target genes, resulting in mRNA degradation or translational suppression [2]. miRNAs regulate more than one-third of human mRNAs, and miRNA expression is

dysregulated in some cancers [3]. Aberrant miRNA expression results in altered regulation of target transcripts and has been implicated in multiple cancer processes, including tumor proliferation and metastasis [4]. Although the specific ways in which aberrant miRNAs modulate NPC development and metastasis remain obscure, and there are many factors that contribute to cancer malignancy, miRNAs have been specifically demonstrated to alter cancer macroautophagy/autophagy [5].

Autophagy, a dynamic catabolic process, where damaged organelles and protein aggregates are engulfed and digested, has been implicated in a wide array of physiological processes and in the pathogenesis of a diverse number of diseases, including cancer [6,7]. Research within the past decade has established that the biological and clinical significance of

**CONTACT** Yiwen You  [yuyiwen\\_nantong@163.com](mailto:yuyiwen_nantong@163.com); Bo You  [youbu19891014@163.com](mailto:youbu19891014@163.com)  Department of Otorhinolaryngology Head and Neck Surgery, Affiliated Hospital of Nantong University, Nantong, Jiangsu Province, China

\*These authors contributed equally to this work

 Supplemental data for this article can be accessed [here](#).

© 2020 The Author(s). Published by Informa UK Limited, trading as Taylor & Francis Group.

This is an Open Access article distributed under the terms of the Creative Commons Attribution-NonCommercial-NoDerivatives License (<http://creativecommons.org/licenses/by-nc-nd/4.0/>), which permits non-commercial re-use, distribution, and reproduction in any medium, provided the original work is properly cited, and is not altered, transformed, or built upon in any way.

autophagy in the context of cancer is dependent on cancer type and genetic background [8]. Considerable evidence has demonstrated that cytoprotective autophagy promotes tumor cell survival by allowing for nutrient uptake [9]. In contrast, autophagy can also exhibit tumor-suppressive effects through a mechanism by which the tumor cells undergo programmed cell death [10,11]. In addition, oncogenic control of autophagy regulation may promote malignant transformation [12]. Autophagy is a complex process that entails the sequential formation of autophagosomes and autolysosomes under the control of autophagy-related (ATG) genes and MAP1LC3B (microtubule associated protein 1 light chain 3 beta proteins) [13]. Notably, miRNAs are characterized as important regulators of autophagy in cancer, and several autophagy-related miRNAs, including *MIR23A*, *MIR29 C*, and *MIR214*, accelerate malignant cancer phenotypes [5,14–17].

*MIR106A-5p*, cytogenetically located on Xq26.2, acts as oncogene and tumor suppressor in different cancers [18,19]. However, the regulatory mechanism underlying the oncogenic effects of *MIR106A-5p* has not been elucidated. We used miRNA microarray to characterize *MIR106A-5p* expression levels in NPC tissues. Clinical data were used to determine the relationship between *MIR106A-5p* and patient outcomes. Subsequent experiments demonstrated the mechanism by which *MIR106A-5p* modulates malignancy and autophagy in NPC. Lastly, we examined how *MIR106A-5p* was upregulated in NPC.

## Results

### Expression and clinical significance of *MIR106A-5p* in NPC

The expression profiles of NPC miRNAs were examined using a combined GEO cohort database (GEO accession number: GSE70970). This data showed that among the differentially expressed miRNAs, *MIR106A-5p* was significantly increased 4.8-fold in NPC tissues (Fig. S1A and S1B). *MIR106A-5p* overexpression was confirmed by quantitative real-time PCR (qRT-PCR) in both NPC tissue and serum samples (Figure 1A and S1D). In addition, *MIR106A-5p* expression was dramatically increased in NPC cell lines, particularly the CNE-2 and 5–8 F lines (Figure 1B). Next, *in situ* hybridization (ISH) with NPC tissue microarrays showed that *MIR106A-5p* overexpression was more prominent in patients with clinical stage IV NPC than in patients with clinical stage I–III NPC (Figure 1C,D), indicating that dysregulation of *MIR106A-5p* may be closely related to terminal stage NPC. This finding was confirmed using a cohort from the GEO database (Fig. S1 C). Further, *MIR106A-5p* upregulation was significantly correlated with NPC recurrence ( $P = 0.048$ , Table S1). Among the 55 patients with recurrence, 98.18% (54/55) developed distant metastases. Together, these data suggest that *MIR106A-5p* serves as a valuable biomarker for predicting advanced cancer or recurrence in NPC. The ISH staining of *MIR106A-5p* was scored as 0–8 (low expression) or 9–16 (high expression) by the X-tile Software, and the survival rate analysis showed that patients with high *MIR106A-5p* expression had worse clinical outcome than patients with low *MIR106A-5p* expression ( $P = 0.0002$ , Figure 1E). TCGA database queries, in agreement with our findings, showed

*MIR106A-5p* overexpression in head and neck cancer (Fig. S1E) that was more prominent in clinical stage IV than stage I–III (Fig. S1 F). *MIR106A-5p* was also a valuable survival biomarker (Fig. S1 G). Overall, these findings indicated that NPC progression is associated with upregulated *MIR106A-5p*.

As *MIR106B-5p* and *MIR106A-5p* belong to the same miRNA family, the expression and role of *MIR106B-5p* in NPC were explored. It was shown that *MIR106B-5p* expression was only elevated in two of four NPC cell lines (Fig. S2A). A series of cellular analyzes found that *MIR106B-5p* does not affect the cell growth and migration of NPC cells (Fig. S2B–S2D).

### *MIR106A-5p* accelerates the malignant NPC phenotype

Since *MIR106A-5p* upregulation was significantly associated with terminal disease stage, recurrence, and poor survival, the direct effects of *MIR106A-5p* on NPC cells were examined. CNE-2 and 5–8 F cells were transfected with *MIR106A-5p* sponges or inhibitor to generate cells with low *MIR106A-5p* expression (Fig. S3A and S3B). The functionality of the *MIR106A-5p* inhibitor was validated by measuring the known target cyclin-dependent kinase inhibitor 1A [20] (Fig. S3 C). Using a series of cellular analyses, we found that NPC cells with decreased *MIR106A-5p* expression had impeded growth and migration capacity (Fig. S3D–I).

Zebrafish and BALB/c mice animal models were used to determine the *in vivo* function of *MIR106A-5p*. First, we injected luciferase-labeled CNE-2 cells with or without knockdown of *MIR106A-5p* into nude mice by tail vein injection, followed by monitoring the tumor growth by measuring the amount of bioluminescence (BLI). We found that the knockdown of *MIR106A-5p* significantly inhibited the metastatic ability of CNE-2 cells (Figure 2A,B). We used a zebrafish tumor model we have recently established for NPC metastasis research [21,22], DiI-labeled CNE2 cells with or without knockdown of *MIR106A-5p* were injected into blastulas, and cells that migrated away from the primary injection site were counted using fluorescence confocal microscopy 8 d after injection. During the experiment, tumor formation and cell survival in zebrafish were monitored by measuring the amount of BLI, and no statistical differences were observed between the two groups before the 8-d cutoff period. However, at 8-d post-injection, the results showed diminished NPC cell migration following *MIR106A-5p* knockdown (Figure 2C,D). These findings were complemented using mouse tumor xenografts where tumor size was measured following subcutaneous injection of high or low *MIR106A-5p*-expressing CNE-2 cells (Figure 2E). Mice injected with cells with low *MIR106A-5p* expression had reduced tumor growth (Figure 2F). Together, these findings provide evidence that *MIR106A-5p* accelerates NPC metastasis and growth. miRNAs are important regulators of autophagy, and loss of autophagy through miRNA disruption modulates tumor development and metastasis. Immunohistochemistry (IHC) analysis showed that xenografts with low *MIR106A-5p* expression had increased MAP1LC3B expression levels (Figure 2F,G), and MAP1LC3B expression levels were negatively correlated with MKI67 (marker of proliferation ki-67) expression in NPC xenografts (Figure 2H). Detection of cleaved CASP3 (caspase 3) expression indicated increased apoptosis in the low *MIR106A-5p*-expression group (Fig. S3 K and S3 L).

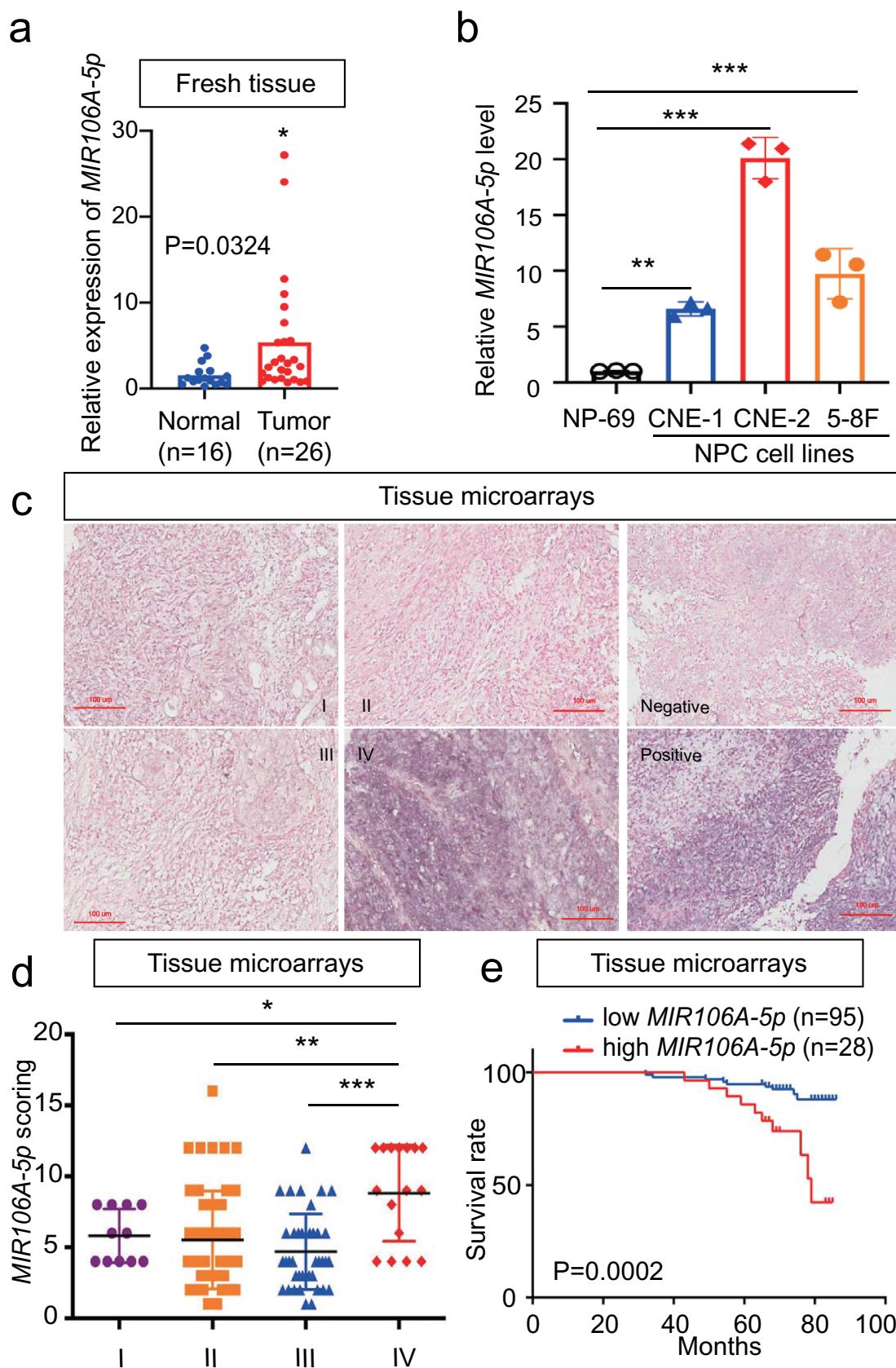


**Figure 1.** Expression and clinical significance of *MIR106A-5p* in NPC. (A) *MIR106A-5p* levels in fresh NPC and non-cancerous nasopharyngeal samples detected by qRT-PCR. P-values were calculated using two-tailed Student's t-tests. (B) *MIR106A-5p* levels in NP-69 and NPC cell lines were examined by qRT-PCR (one-way ANOVA). CNE-1, CNE-2, 5-8 F, and 6-10B are human NPC cell lines; NP-69 is an immortalized normal nasopharyngeal epithelial cell line. (C) Representative *MIR106A-5p* ISH staining of NPC tissue microarrays, scale bar: 100  $\mu$ m. (D) Statistical comparison of *MIR106A-5p* expression across clinical stages using one-way ANOVA. (E) The ISH staining score of *MIR106A-5p* in NPC tissue microarrays was defined as low expression (scores of 0–8) or high expression (scores of 9–16) by the X-tile Software. Then Kaplan-Meier analysis was used to compare overall survival using the log-rank test. All experiments were conducted with three independent replicates. All graphs show mean  $\pm$  SEM of at least three independent experiments. \* $P < 0.05$ , \*\* $P < 0.01$ , \*\*\* $P < 0.001$ .



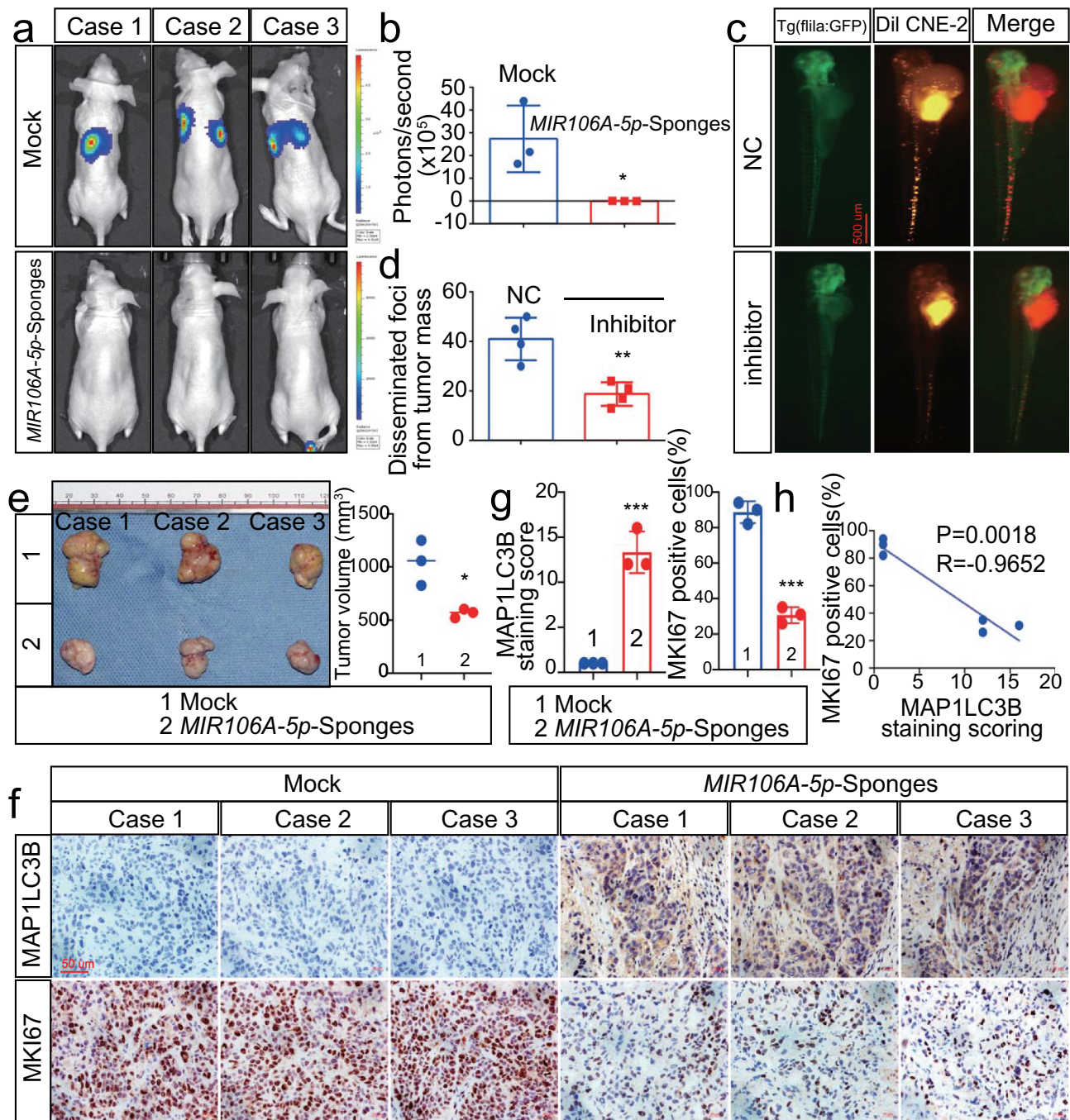


**Figure 2.** Silencing of *MIR106A-5p* inhibits NPC proliferation and migration *in vivo*. (A) Visualization of lung metastasis after intravenous injection of CNE-2 cells, with or without knockdown of *MIR106A-5p*, in BALB/c mice. Representative images of bioluminescence signals and normalized photon flux are shown. (B) Graph representing mean intensity of fluorescence 7 weeks after tumor injection (\* $P < 0.05$ , t-test). (C) CNE2 cells transfected with *MIR106A-5p* inhibitor and labeled with Dil were injected into the perivitelline space of zebrafish embryos. Migration of CNE2 cells was measured using fluorescence microscopy at day 8 post-injection. (D) Quantification of migratory cell numbers and analysis using Student's t-test (\*\* $P < 0.01$ ). (E) Cells with stable silencing of *MIR106A-5p* or control cells were subcutaneously transplanted in nude mice ( $n = 3$  per group). Subcutaneous tumor volumes at day 21 are shown (\* $P < 0.05$ , t-test). (F) Immunohistochemistry (IHC) analysis of tumor MAP1LC3B and MKI67 expression across tumor groups. Scale bar: 50  $\mu\text{m}$ . Quantification of IHC staining for MAP1LC3B and MKI67 expression using Student's t-test (\*\* $P < 0.001$ ) (G) and Pearson correlation between MAP1LC3B and MKI67 expression (H). Linear regression. All experiments were repeated three times. Data represent mean  $\pm$  SEM.

### MIR106A-5p suppresses autophagy in NPC cells

Based on these IHC results, we hypothesized that dysregulated *MIR106A-5p* expression might influence autophagy. Therefore, the effect of *MIR106A-5p* on autophagosome and autolysosome generation was

evaluated. Of note, silencing *MIR106A-5p* expression markedly promoted expression of ATG genes and induced autophagic flux to generate autophagosomes and/or autolysosomes (Figure 3A,I), indicating that *MIR106A-5p* potentially inhibits autophagy in NPC cells.



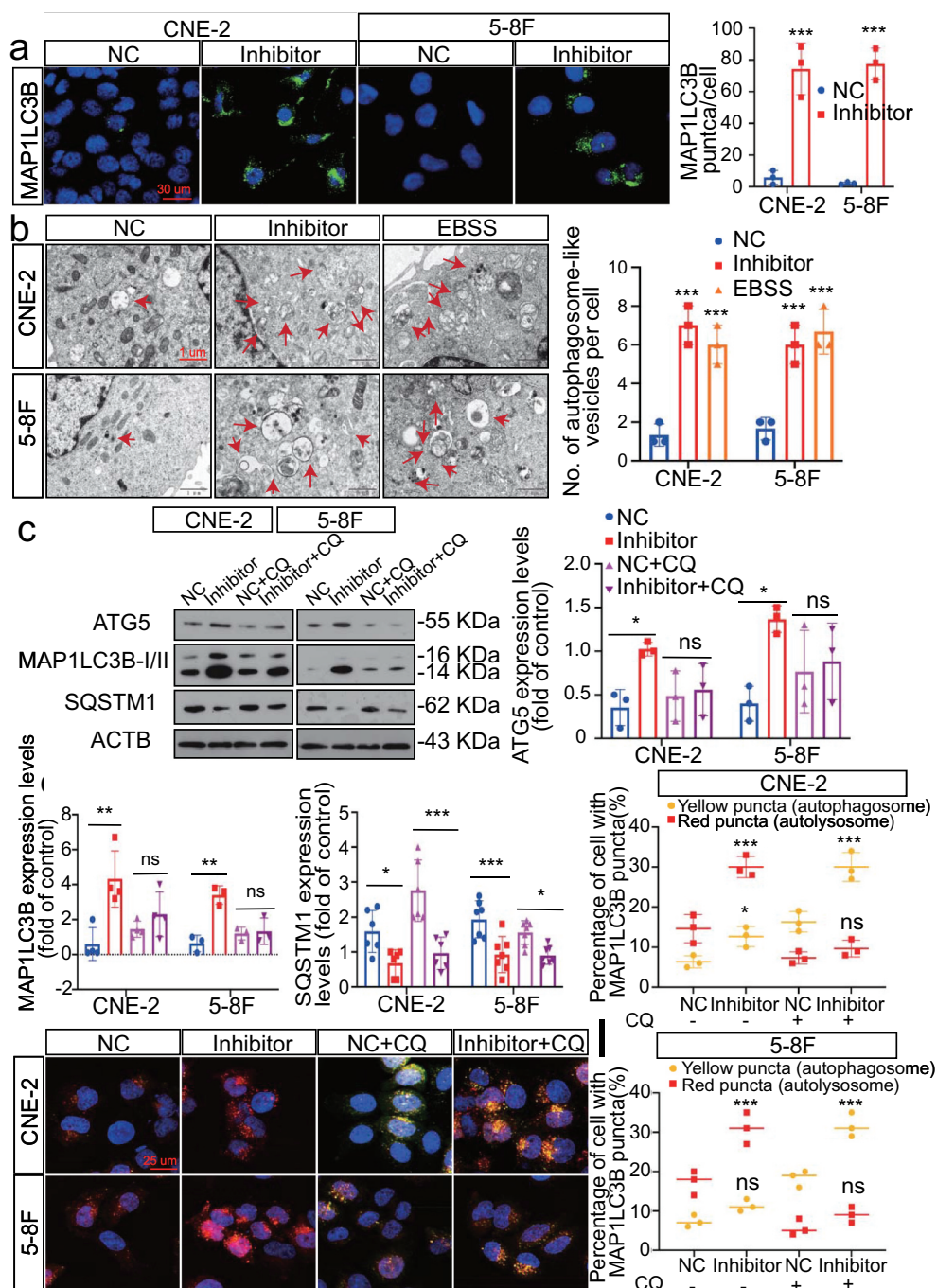


**Figure 3.** Silencing of *MIR106A-5p* promotes autophagy in NPC cells. (A) Left, immunofluorescence analysis of endogenous MAP1LC3B puncta in cells transfected with *MIR106A-5p* inhibitor or control. Right, total number of endogenous MAP1LC3B puncta per cell. Student's t-test. (B) Left, transmission electron microscopy analysis of autophagy. Arrows indicate cell autophagosomes/autolysosomes. Right, quantification of the total autophagosome numbers per cell analyzed using Student's t-tests. EBSS: Earle's balanced salt solution. (C) Western blot (WB) analysis of changes in MAP1LC3B conversion, ATG5, and SQSTM1 levels induced by *MIR106A-5p* silencing in NPC cells in the absence (–) or presence (+) of 10  $\mu\text{mol/L}$  chloroquine (CQ) treatment. ACTB was used as a loading control. (D–F) quantification of WB results from three independent experiments. (G–I) Cells were transiently transfected with mRFP-GFP-MAP1LC3B reporter, which differentiates between autophagosomes (GFP<sup>+</sup>RFP<sup>+</sup>, yellow puncta) and autolysosomes (GFP<sup>+</sup>RFP<sup>+</sup>, red puncta). Cells were transfected with *MIR106A-5p* inhibitor in the absence or presence of CQ to inhibit autophagosome and lysosome fusion. Results were analyzed using two-way ANOVA with at least three independent replicates per condition. All experiments were repeated three times with similar results. Images in A–I are representative of three independent experiments. Data represent mean  $\pm$  SEM. Unprocessed original scans of three independent blots are shown in Fig. S9.

### **MIR106A-5p accelerates the NPC malignant phenotype by suppressing autophagy**

The function of *MIR106A-5p*-suppressed autophagy in NPC development and metastasis was examined by assessing the growth and migration capacities of cells following knockdown of ATG5.

Knocking down ATG5 significantly decreased the autophagy induced by *MIR106A-5p* inhibition (Figure 4A). Since three-dimensional cell culture models more closely mimic the *in vivo* tumor microenvironment, three-dimensional NPC cell cultures were used to assess cell viability and proliferation. Silencing *MIR106A-5p* expression reduced spheroid formation and cell

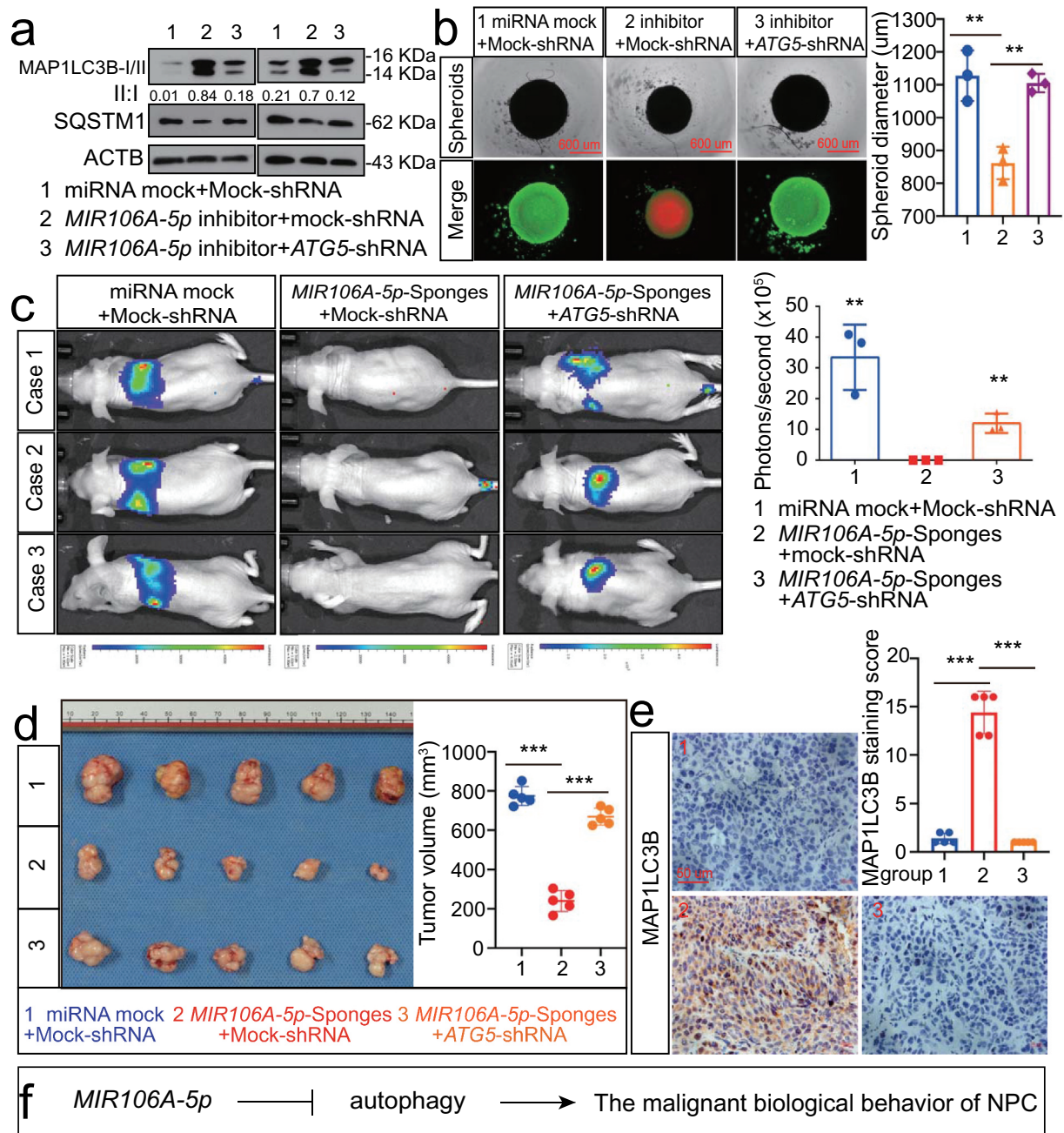


**Figure 4.** Blocking autophagy induced by *MIR106A-5p* inhibitor rescues NPC proliferation and migration. (A) WB analysis of MAP1LC3B-I, MAP1LC3B-II and SQSTM1 in cells transfected with *MIR106A-5p* inhibitor along with transfection of lentiviral ATG5-shRNA or mock vector. (B) Left, cell growth and viability analysis via three-dimensional spheroid formation assay. Red fluorescence represents dead cells and green fluorescence represents live cells. Right, spheroid diameter analyzed using one-way ANOVA (\*\*P < 0.01, scale bar: 600 μm). (C) Left, visualization of lung metastasis after intravenous injection of stated cells. Right, mean intensity of fluorescence (\*\*P < 0.01, one-way ANOVA). (D) Left, representative NPC xenografts in mice for indicated groups (n = 5 per group). Right, tumor volumes on day 21. (E) Tumors were analyzed by IHC for MAP1LC3B expression using one-way ANOVA. Scale bar: 50 μm. (F) Schematic diagram. All experiments were repeated three times. Data represent mean ± SEM. Images in A-B and E are representative of three independent experiments. All spheroid formation for three independent experiments in B and IHC images for every subcutaneous tumor in E are shown in Fig. S8. Unprocessed original scans of three independent blots are shown in Fig. S9.

viability, and this phenotype was partially rescued by knocking down ATG5 (Figure 4B). Moreover, the decreased metastasis and growth induced by *MIR106A-5p* sponges *in vivo* was abolished following knockdown of ATG5 (Figure 4C-E). These findings indicate that *MIR106A-5p*-suppressed autophagy accelerates malignant NPC phenotypes (Figure 4F).

#### **BTG3 is the direct target of *MIR106A-5p* and correlates with poor prognosis in head and neck cancer**

Autophagy-related targets of *MIR106A-5p* were identified using four common bioinformatics tools to generate a pool of predicted candidate genes (Figure 5A,B). Detailed information of the target-gene scan is provided in Table S2. Among these



targets, *BTG3* (BTG anti-proliferation factor 3) was selected due to the potentially high-affinity binding sites of *MIR106A-5p* (Figure 5C) and its role in regulating autophagy [23]. Luciferase reporter assays showed biologically effective interactions between *MIR106A-5p* and the *BTG3* 3'-UTR (Figure 5D). In addition, *BTG3* mRNA and BTG3 protein expression were decreased in NPC (Figure 5E, S5A and S5B). Interestingly, the BTG3 protein levels dramatically increased following *MIR106A-5p* inhibition, while *BTG3* mRNA levels remained unchanged (Figure 5F-I). Of note, *MIR106A-5p* expression negatively correlated with BTG3 protein levels in NPC tissue microarrays (Figure 5J), whereas no inverse correlation was observed between *MIR106A-5p* and *BTG3* mRNA levels in NPC tissues and TCGA database (Fig. S4A and S4B). These results indicated that *MIR106A-5p* might regulate BTG3 expression through translational suppression. Finally, Kaplan-Meier analysis revealed that low BTG3 levels were associated with worse clinical outcomes in NPC tissue microarrays ( $P = 0.029$ , Figure 5K) and TCGA database ( $P = 0.003$ , Fig. S1 H). Collectively, these data suggest that *MIR106A-5p* directly regulates autophagy by targeting BTG3.

### ***BTG3 is essential for the suppression of autophagy by MIR106A-5p***

Regulation of autophagy by BTG3 was determined through transfection experiments. Overexpression of BTG3 markedly increased induction of autophagy, which was consistent with the increased expression of ATGs (Fig. S5 C) and significant accumulation of autophagosomes and autolysosomes (Fig. S5 C and S5D). We showed that BTG3 was involved in the *MIR106A-5p*-associated inhibition of autophagy by transfecting NPC cells with siRNA against *BTG3* (Figure 6A-E). A series of analyses demonstrated that knockdown of BTG3 abolished the capacity of *MIR106A-5p* inhibition to increase autophagy (Figure 6A-E), providing evidence that the suppression of autophagy by *MIR106A-5p* is dependent on its ability to decrease BTG3 levels. Additionally, immunofluorescence (IF) co-staining of *MIR106A-5p*, MAP1LC3B, and BTG3 was performed to show the *MIR106A-5p*-BTG3-MAP1LC3B signaling cascade (Fig. S5 F).

### ***BTG3 is essential for MIR106A-5p to accelerate malignant NPC phenotypes***

To further corroborate that the *MIR106A-5p*-BTG3 axis results in accelerated malignancy, NPC cells treated with *MIR106A-5p* sponges were transduced with lentiviral *BTG3*-shRNA (Fig. S5E and 7A-7E). *MIR106A-5p* inhibition reduced metastasis and growth of NPC cells, but these effects were significantly diminished following BTG3 knockdown (Figure 7A-E and S6A-S6E). IHC analysis showed that autophagy was also reduced in the NPC xenograft group with accelerated malignant phenotype (Figure 7F-K), suggesting that the autophagy-suppressive

and tumor-promoting effects of *MIR106A-5p* require BTG3 (Figure 7L).

### ***The MIR106A-5p-BTG3 axis suppresses autophagy via the MAPK pathway***

We next sought to identify BTG3-interacting partners involved in *MIR106A-5p*-induced autophagy. GST affinity-isolation assay was performed, which identified 253 BTG3-binding proteins (Fig. S7A). A detailed list of the binding proteins is provided in Table S3. There were no previously reported autophagic proteins among these interacting partners. To further investigate the mechanism by which BTG3 regulates autophagy, we focused on the autophagy-related pathways. Following KEGG pathway analysis of *MIR106A-5p* targets, the MAPK and AKT-MTOR pathways emerged as negative modulators of autophagy [24] (Fig. S7B). Therefore, rescue experiments using inhibitors of these pathways were performed to investigate the relative contributions of these pathways to *MIR106A-5p*-BTG3-mediated tumor progression. We found that only suppression of MAP2K1/MEK activity with PD184352 significantly inhibited the cellular proliferation and migration induced by *MIR106A-5p* and *BTG3* silencing; by contrast, inhibition of AKT activity by MK2206 failed to alter *MIR106A-5p*-BTG3-mediated tumor growth and migration (Figure 8A-D). MAPK signaling pathway PCR array analyses revealed expression level changes following *MIR106A-5p* silencing. The identities and heatmap data of 86 selected genes are shown in Fig. S11B. Overall, silencing of *MIR106A-5p* significantly reduced *ATF2*, *CCNB2*, *CREB1*, *ETS2*, *KRAS*, *KSR1*, *MAP3 K4*, *MAPK1*, *MAPK6*, *MAPKAPK3*, *MYC*, and *RAC1* expression (Fig. S7 C and S7D). Furthermore, we examined whether *MIR106A-5p*-BTG3 axis-dependent autophagy inhibition in NPC resulted from activation of MAPK signaling. p-MAP2K1 and downstream p-MAPK1/ERK and p-MTOR levels were decreased when *MIR106A-5p* inhibition or BTG3 expression activated autophagy. After suppression of MAP2K1 activity with PD184352, p-MAP2K1, p-MAPK1, and p-MTOR levels and ATG expression were rescued in *MIR106A-5p* and BTG3 knockdown cells (Figure 8E), suggesting that activated MAPK signaling is partially responsible for the suppression of autophagy by the *MIR106A-5p*-BTG3 axis in NPC.

### ***MIR106A-5p upregulation in NPC results from increased transactivation by EGR1 and SOX9***

We then examined how *MIR106A-5p* was upregulated in NPC. Sequence analysis of the *MIR106A-5p* promoter identified putative binding sites for EGR1 (early growth response 1) and SOX9 (SRY-box transcription factor 9) at -136 and -1472, respectively (Figure 9A), suggesting that EGR1 and SOX9 regulate the transcription of *MIR106A-5p*. Notably, EGR1 and SOX9 were both upregulated in the NPC cell lines (Figure 9B). Silencing EGR1 and SOX9

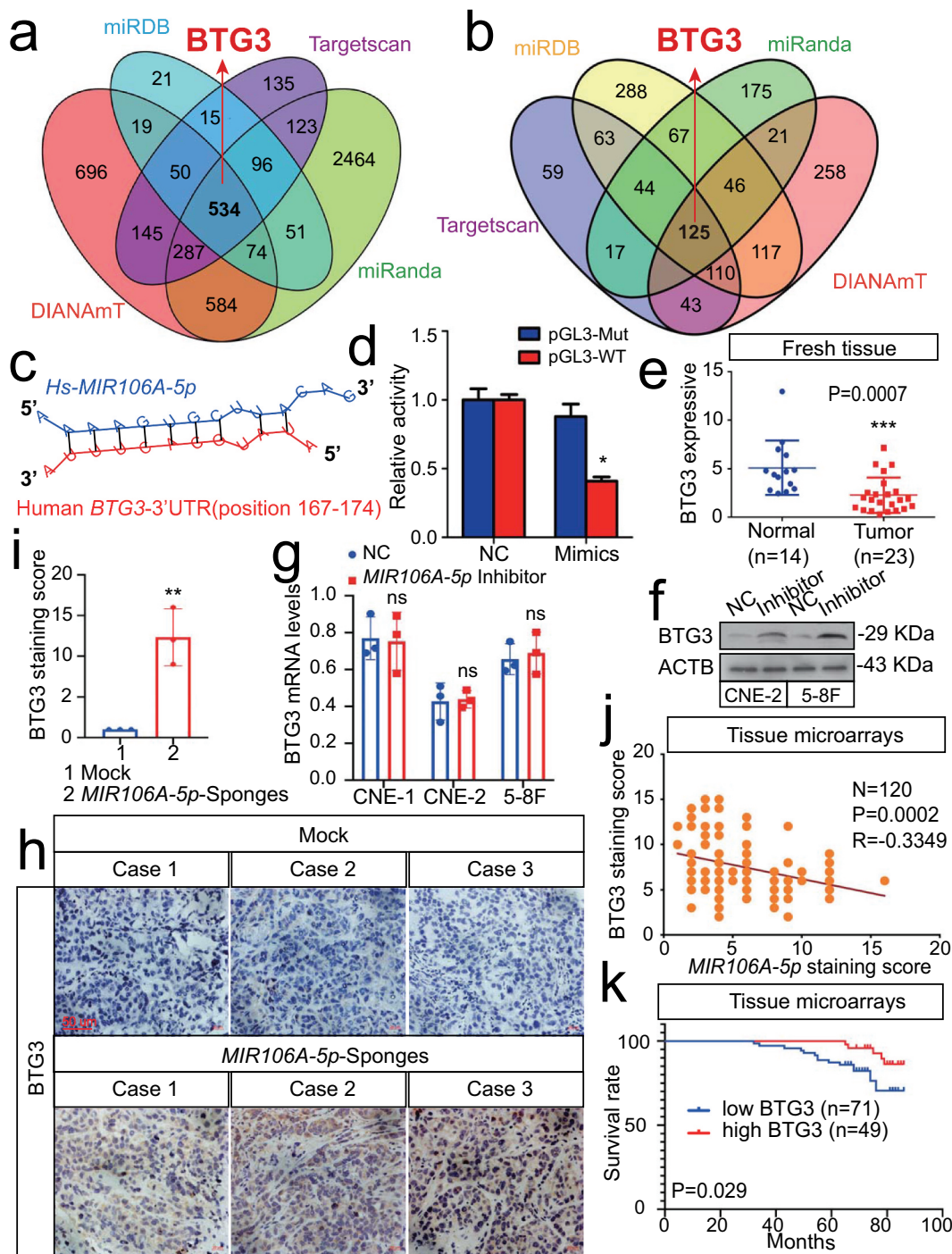


**Figure 5.** *MIR106A-5p* directly targets *BTG3*. (A) Venn diagram depicting predicted *MIR106A-5p* targets. (B) Venn diagram depicting *MIR106A-5p* targets with high target scores. (C) Schematic of predicted *MIR106A-5p* binding sequences in the 3'-UTR of *BTG3*. (D) *MIR106A-5p* overexpression reduced wild-type *BTG3* 3'-UTR luciferase activity but not mutant *BTG3* 3'-UTR luciferase activity (analyzed using Student's t-test). (E) *BTG3* levels in fresh NPC and non-cancerous nasopharyngeal samples detected by qRT-PCR. P-values were calculated using two-tailed Student's t-tests. (F) WB analysis of changes in *BTG3* levels induced by *MIR106A-5p* silencing. (G) qRT-PCR analysis of changes in *BTG3* levels induced by *MIR106A-5p* silencing. (H) Representative IHC images of *BTG3* staining in tissues collected from two groups of NPC xenografts. Scale bar: 50  $\mu$ m. (I) Quantification of IHC staining for *MAP1LC3B* expression using Student's t-test (\*\* $P < 0.01$ ). (J) IHC staining of *BTG3* expression in NPC tissue microarrays. Pearson correlation between *BTG3* and *MIR106A-5p* expression was analyzed. (K) The ISH staining score of *BTG3* in NPC tissue microarrays was defined as low expression (scores of 0–7) or high expression (scores of 8–16) by the X-tile Software. Kaplan-Meier analysis was used to compare overall survival using the log-rank test. All experiments were conducted with three independent replicates. All graphs show mean  $\pm$  SEM of at least three independent experiments. Unprocessed original scans of three independent blots for F are shown in Fig. S9.

expression decreased *MIR106A-5p* levels, and overexpression of *EGR1* and *SOX9* increased *MIR106A-5p* levels (Figure 9C-E and S7E-S7 G). Furthermore, luciferase reporter assay and chromatin immunoprecipitation (ChIP) analysis showed that both *EGR1* and *SOX9*

directly bound to the predicted binding sites of the *MIR106A-5p* promoter and transactivated *MIR106A-5p* (Figure 9F-H). Correlation between *SOX9* and *MIR106A-5p* expression in NPC tissues using IHC and ISH assay show that *SOX9* expression was positively correlated to



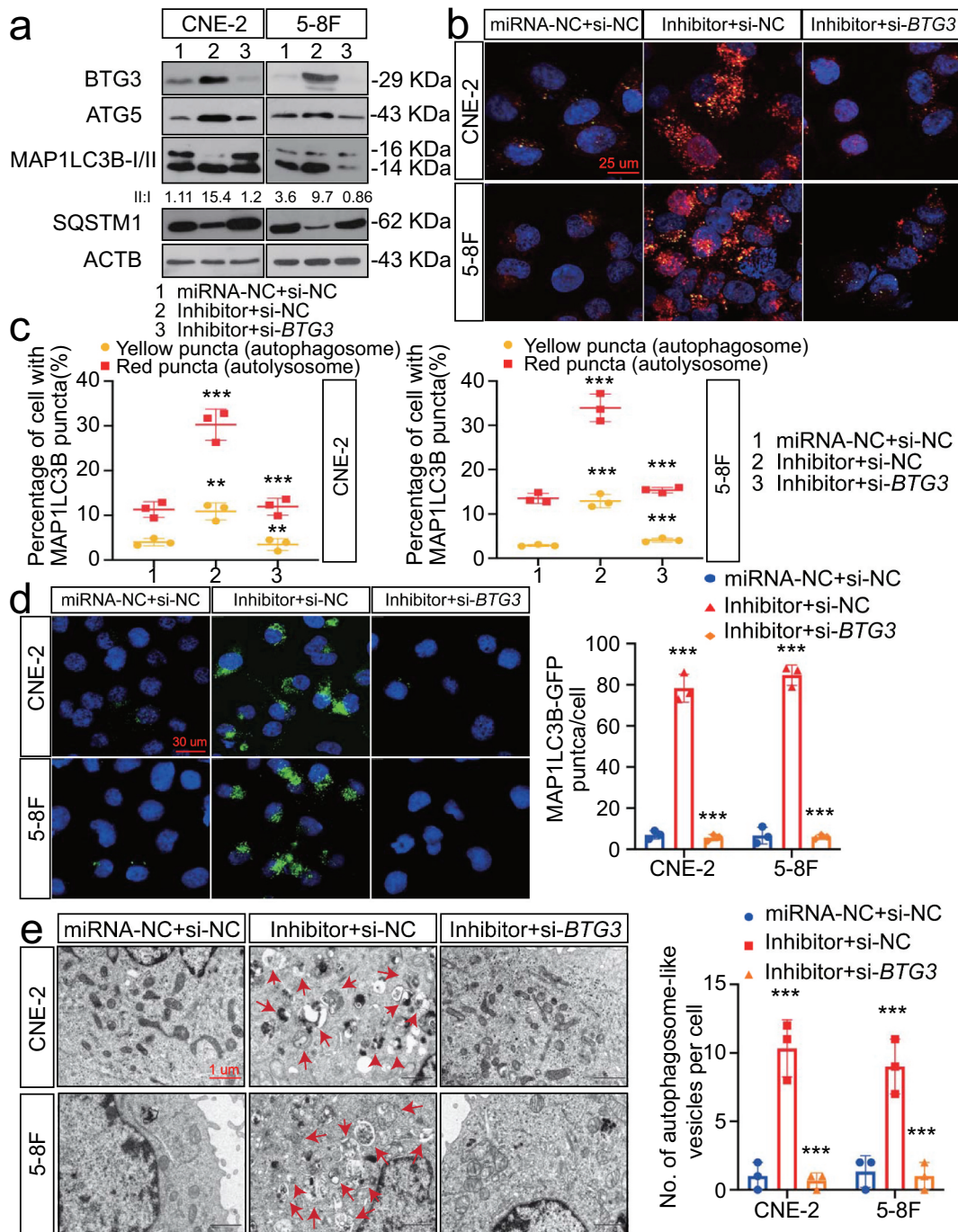


**Figure 6.** The *MIR106A-5p*-BTG3 axis regulates NPC cell autophagy. (A) Expression of MAP1LC3B conversion, ATG5, and SQSTM1 was measured by WB in *MIR106A-5p*-silenced NPC cells transfected with *BTG3*-specific siRNA or control. (B) Detection of autophagic flux with the mRFP-GFP-LC3 reporter in *MIR106A-5p*-silenced NPC cells transfected with *BTG3*-specific siRNA or control. Scale bar: 25  $\mu$ m. (C) Analysis of autophagic flux using two-way ANOVA with at least three independent replicates per condition (\*\* $P < 0.01$ , \*\*\* $P < 0.001$ ). (D) Left, immunofluorescence analysis of endogenous MAP1LC3B puncta in cells. Scale bar: 30  $\mu$ m. Right, total number of endogenous MAP1LC3B puncta per cell analyzed using two-way ANOVA with at least three independent replicates per condition (\*\*\* $P < 0.001$ ). (E) Left, transmission electron microscopy analysis of autophagy. Arrows, autophagosomes/autolysosomes. Scale bar: 1  $\mu$ m. Right, the total numbers of autophagosomes per cell were quantified and analyzed using two-way ANOVA with at least three independent replicates per condition (\*\*\* $P < 0.001$ ). Experiments were conducted with at least three independent replicates. All experiments were repeated three times with similar results. Images in A-B and D-E are representative of three independent experiments. Data represent mean  $\pm$  SEM. Unprocessed original scans of three independent blots are shown in Fig. S9.

*MIR106A-5p* levels (Figure 9I). Survival analysis of NPC tissue microarrays further showed that NPC patients with high SOX9 expression had poor prognosis when compared to those with low SOX9 expression (Figure 9J).

GEO cohort database and TCGA database analysis also confirmed these prognostic findings (Figure 9K and S11). These results showed that *MIR106A-5p* overexpression in NPC results from increased transactivation by EGR1 and

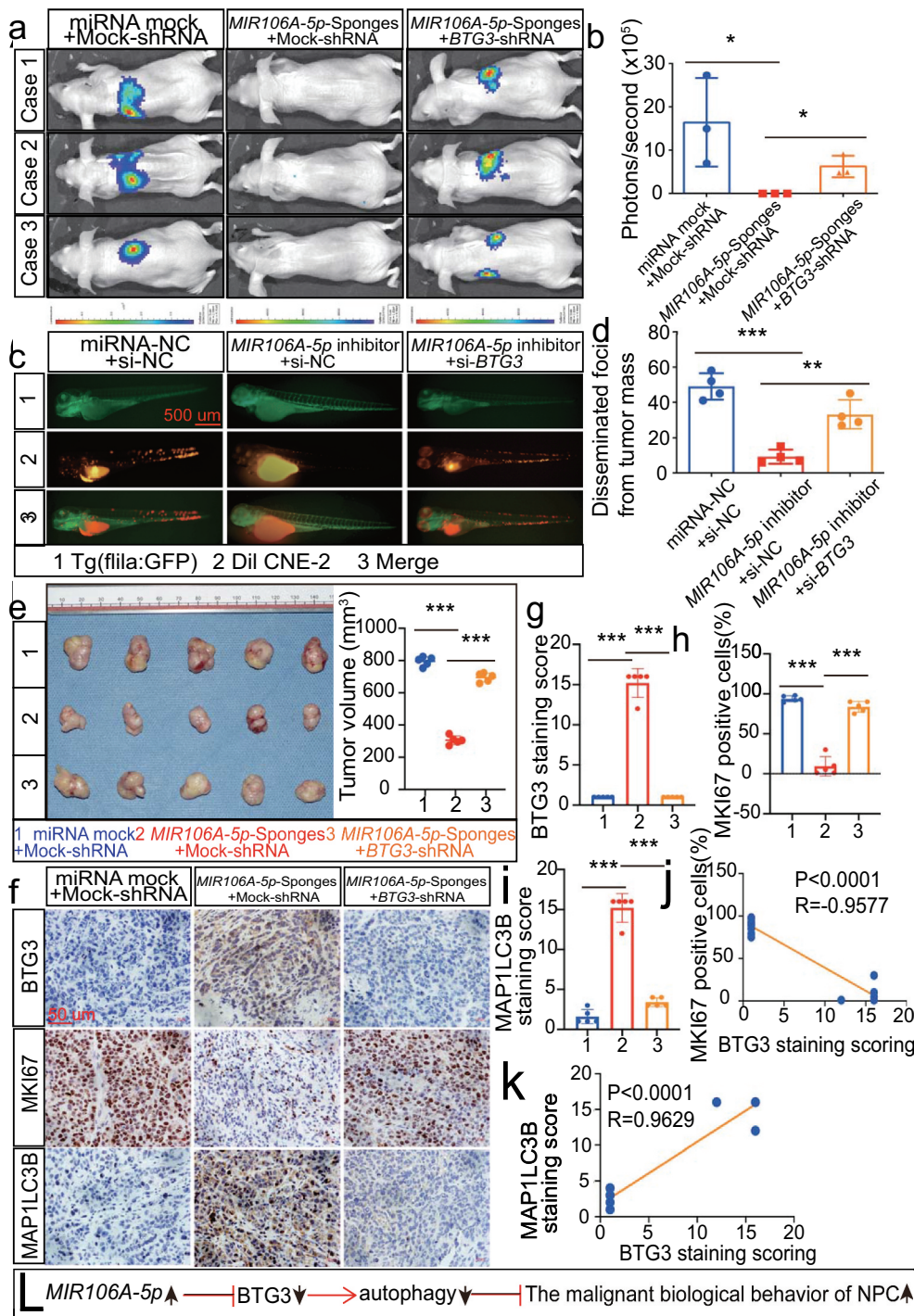


**Figure 7.** The *MIR106A-5p*-BTG3 axis regulates proliferation and migration in NPC cells. (A) *MIR106A-5p*-silenced NPC cells were transfected with lentiviral *BTG3*-shRNA or control and inoculated into nude mice by tail vein injection. Visualization of lung metastasis in different groups are representative of three independent experiments. (B) Graph representing the mean intensity of fluorescence ( $*P < 0.05$ , one-way ANOVA). (C) *MIR106A-5p*-silenced NPC cells were transfected with *BTG3*-siRNA or control and labeled with Dil. Labeled cells were injected into the perivitelline space of zebrafish embryos to detect tumor cell metastasis by fluorescence microscopy. (D) Quantification of migratory cell numbers ( $**P < 0.01$ ,  $***P < 0.001$ , one-way ANOVA). (E) Left, representative NPC xenografts in mice for indicated groups ( $n = 5$  per group). Right, tumor volumes on day 21. (F) Tumors were analyzed by IHC for BTG3, MKI67, and MAP1LC3B expression using one-way ANOVA. Scale bar: 50  $\mu$ m. Quantification of IHC staining for BTG3 (G), MKI67 (H), and MAP1LC3B (I) expression using one-way ANOVA ( $***P < 0.001$ ). (J) Pearson correlation between BTG3 and MKI67 expression and (K) MAP1LC3B and BTG3 expression. Linear regression. (L) Schematic diagram. All experiments were repeated three times. Data represent mean  $\pm$  SEM. All IHC images for every subcutaneous tumor in F are shown in Fig. S8.

SOX9. A schematic overview of the mechanism by which *MIR106A-5p* autophagy modulation promotes malignant phenotypes is displayed in Figure 9L.

## Discussion

Previous reports have identified altered miRNA expression in NPC, including instances of decreased expression of tumor-



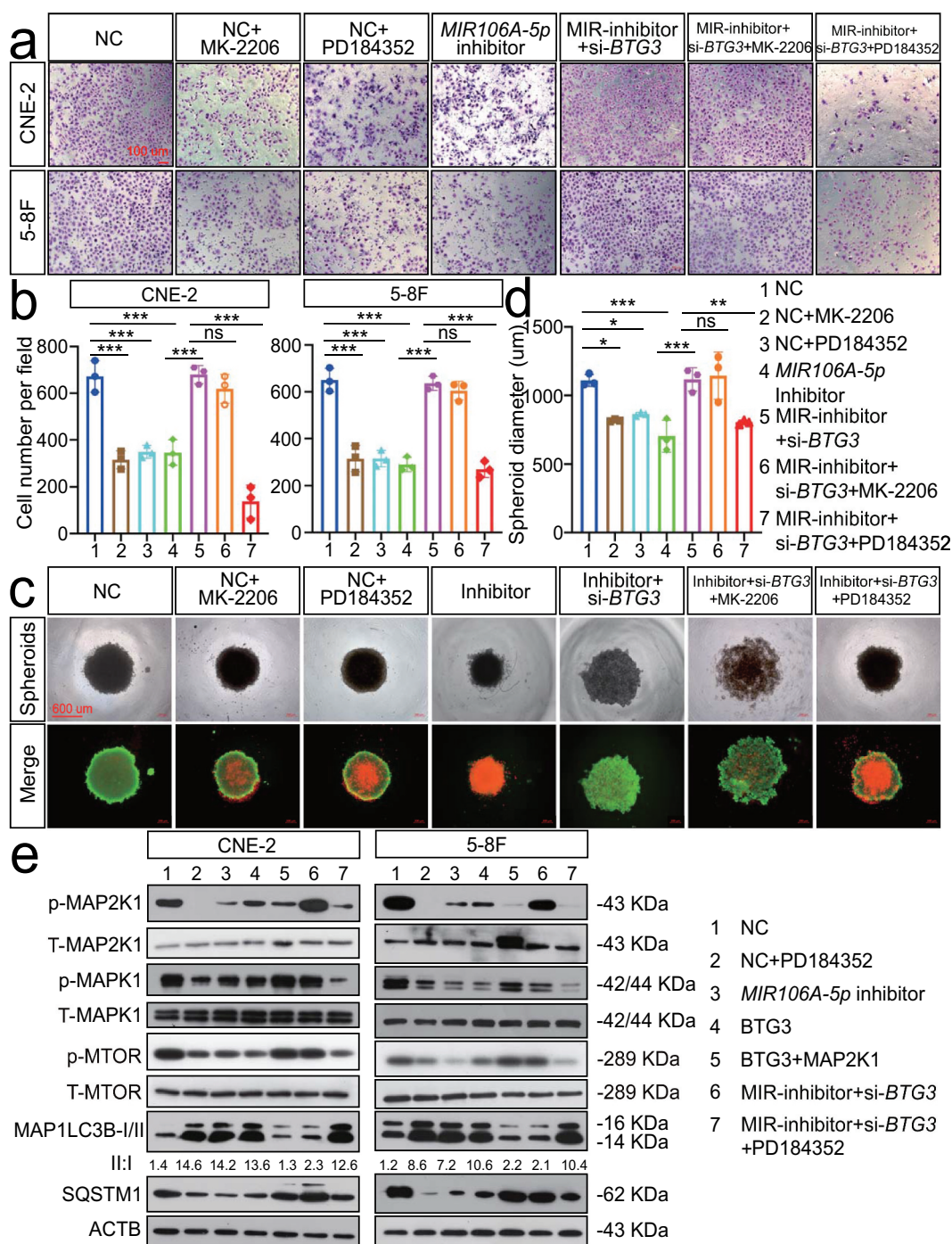


**Figure 8.** The *MIR106A-5p*-BTG3 axis regulates NPC cell autophagy by activating MAPK signaling. Rescue experiments with Transwell assay (A-B) and three-dimensional spheroid formation assay (C-D) were performed using inhibitors of AKT and MAPK signaling using *MIR106A-5p*-silenced NPC cells transfected with *BTG3*-specific siRNA or control. MK2206: AKT inhibitor. PD184352: MAP2K1 inhibitor. (B) The number of cells that invaded through the membrane was counted in 3 fields per group with three independent replicates (\*\*\*\*P < 0.001, one-way ANOVA). Data represent mean  $\pm$  SEM. (D) Spheroid diameters were analyzed using one-way ANOVA (\*P < 0.05, \*\*P < 0.01, \*\*\*\*P < 0.001, scale bar: 600  $\mu$ m). (E) Rescue experiments with WB analysis of p-MAP2K1/MAP2K1, p-MAPK1/MAPK1, and p-MTOR/MTOR levels, as well as autophagy-related gene levels, in different conditions in NPC cells. PD184352: MAP2K1 inhibitor, BTG3: BTG3 overexpression vector, MAP2K1: MAP2K1 overexpression vector. All experiments were repeated three times with similar results. Images in A, C, and E are representative of three independent experiments. Data represent mean  $\pm$  SEM. All spheroid formation images of three independent experiments in C are shown in Fig. S8. Unprocessed original scans of three independent blots are shown in Fig. S9.

suppressive and increased expression of oncogenic miRNAs [25]. The differentially expressed miRNA profiles of NPC in a cohort from the GEO database (GSE70970) showed that 97 miRNAs had significantly altered expression. Among them, 21 were EBV-related miRNAs, 20 of which have been

previously reported to be involved in NPC progression. Among the remaining differentially expressed miRNAs, the miR-17 ~ 106 family, including *MIR17*, *MIR106A* and *MIR106B*, had significantly increased expression and drew our attention. The miR-17 ~ 106 family is reported to

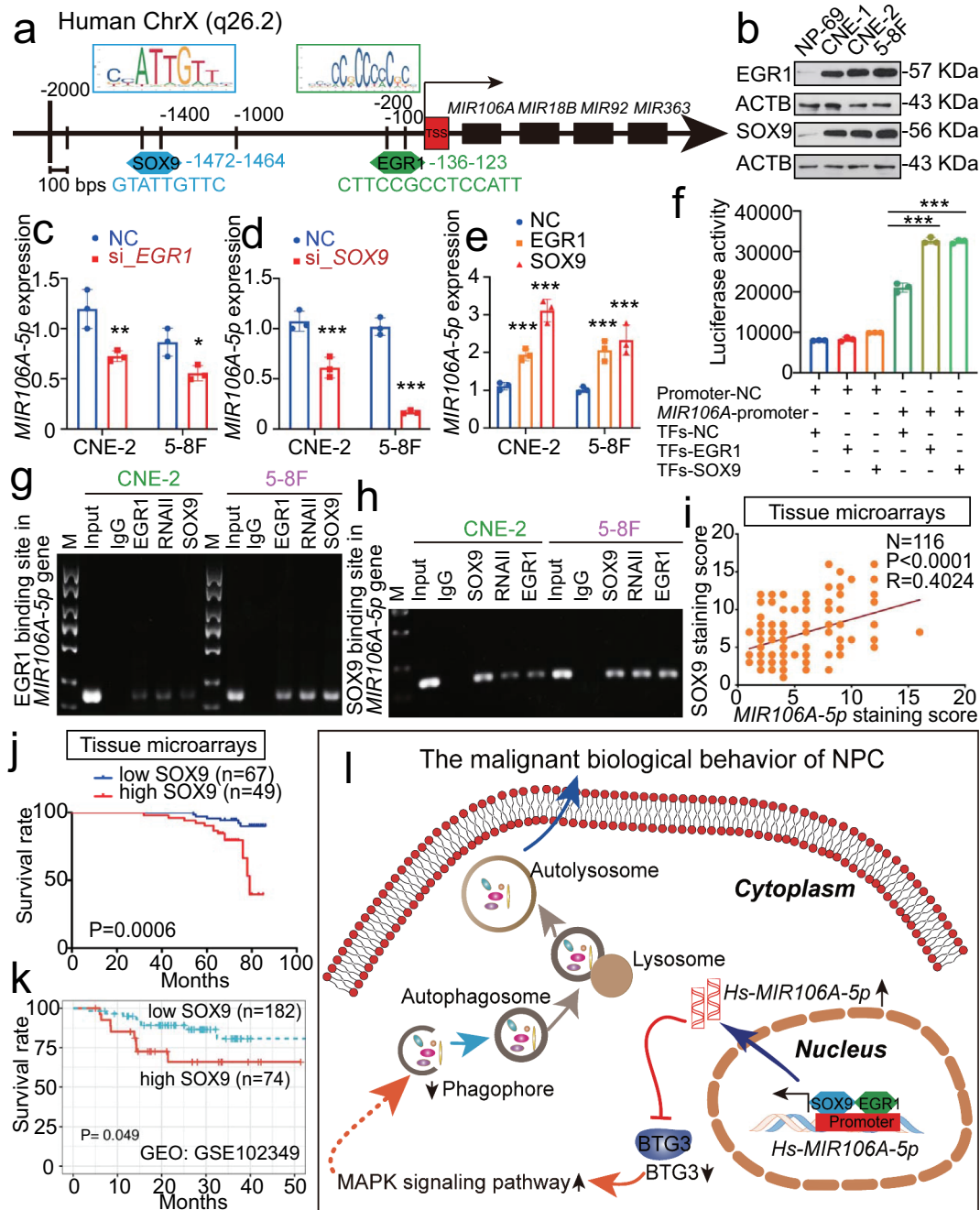


**Figure 9.** *MIR106A-5p* overexpression in NPC results from increased transactivation by EGR1 and SOX9. (A) Schematic diagram of predicted EGR1 and SOX9 binding sequences within a region 136 bp and 1472 upstream of the *MIR106A-5p* gene locus TSS. (B) Immunoblotting analysis of EGR1 and SOX9 in NP-69 and NPC cells. qRT-PCR analysis of *MIR106A-5p* expression after EGR1 (C) and SOX9 (D) knockdown or EGR1 and SOX9 overexpression (E). (F) Binding of transcription factors (EGR1 and SOX9) to the *MIR106A-5p* promoter in NPC cells was confirmed by dual-luciferase reporter assays. (G-H) ChIP assays were performed to determine the binding of both EGR1 and SOX9 to the *MIR106A-5p* promoter region in NPC cells. (I) IHC analysis of SOX9 expression in NPC tissue microarrays and correlation between *MIR106A-5p* expression levels and SOX9 staining score using Spearman's rank correlation analysis. Kaplan-Meier analysis of the association of SOX9 expression was used to estimate survival time in NPC patients (J) and a GEO database cohort (accession number GEO: GSE102349) (K); differences in survival were analyzed using the log-rank test. (L) Schematic overview of the role of *MIR106A-5p* in promoting the malignant phenotype in NPC by modulating autophagy. *MIR106A-5p* targets BTG3 to activate MAPK signaling, which accelerates malignant NPC phenotypes by autophagy suppression. *MIR106A-5p* overexpression in NPC results from increased transactivation by EGR1 and SOX9. Experiments were conducted with at least three independent replicates. Data represent mean  $\pm$  SEM. One-way ANOVA was used for statistical analysis (\* $P < 0.05$ , \*\* $P < 0.01$ , \*\*\* $P < 0.001$ ).

participate in multiple cancer cellular processes as oncogenic factors in a variety of tumor types [26–28]. Several studies have suggested that *MIR17* is involved in the development and tumorigenesis of NPC [29,30]; however, the expression

and role of *MIR106A/MIR106B* in NPC have not been elucidated. Like previous studies suggesting that *MIR106A-5p* has tumor-promoting roles in hepatocellular carcinoma, colorectal cancer, and ovarian cancer [31–33], this study showed that



*MIR106A-5p* was significantly overexpressed and served as an oncogene in NPC.

NPC patients with cancers detected at an early stage can be effectively cured using standard therapies, but the prognosis of patients with advanced-stage disease is extremely poor. Following recurrence, therapy often fails, and advanced stage and recurrent NPC present a challenge to clinicians. This study showed that *MIR106A-5p* overexpression was significantly higher in patients with clinical stage IV and that *MIR106A-5p* levels significantly correlated with recurrence. These findings suggest the prognostic utility of *MIR106A-5p* levels in discrimination of terminal stage and risk of recurrence in NPC patients. Therefore, quantification of *MIR106A-5p* levels before initiation of therapy may predict the odds of recurrence and survival and would complement TNM staging.

Autophagy plays an intricate and context-dependent role in different cancer types [34]. Autophagy is considered to be a tumor-suppressive mechanism in NPC. Lin et al. [35] demonstrated that the autophagy machinery in NPC contained mutations and deletions in three critical autophagy genes, *ATG2A*, *ATG7*, and *ATG13*, suggesting low levels of autophagy in NPC. In parallel, there is published evidence showing that autophagy defects and high SQSTM1 (sequestosome 1) expression can facilitate epithelial to mesenchymal transition in NPC and promote metastasis [36,37]. In addition, autophagy deficiency in NPC is significantly correlated with chemotherapy and radiotherapy resistance [38,39]. Studies of NPC have identified autophagy inactivation as a consequence of dysregulation of SQSTM1, ANXA1, angiotensin-(1-7), and SSRP1 (structure specific recognition protein 1) [36,37,40,41]; however, how miRNAs regulate autophagy and the impact of miRNA-regulated autophagy on NPC malignancy are unclear [42]. Previous studies reported that *ATG7* and *RUNX1* are targets of *MIR106A-5p* [43–45], and both *ATG7* and *RUNX1* are known to participate in autophagy regulation [46]. Therefore, we directly explored the role of *MIR106A-5p* in autophagy and the role of autophagy in NPC malignancy. This study showed that *MIR106A-5p* strongly impeded NPC autophagy, which in turn promoted pro-tumorigenic phenotypes.

In this study, we identified BTG3 as a new direct target of *MIR106A-5p* for its anti-autophagic effect and tumor-promoting function in NPC. Although several known targets of *MIR106A-5p*, such as *ATG7* and *RUNX1*, have been reported to regulate autophagy, this is the first report of *MIR106A-5p* directly regulating autophagy by targeting BTG3. Tumor-suppressive functions of BTG3 have been reported [23,47], although not in the context of NPC. Gou et al. found that BTG3 overexpression increased MAP1LC3B and BECN1 expression in gastric cancer, indicating that BTG3 may regulate autophagy, but these findings were not further investigated [23]. Paradoxically, *MIR106A-5p* expression was negatively correlated with BTG3 protein levels, but there was no inverse correlation between *MIR106A-5p* and *BTG3* mRNA levels. Although we discovered that *MIR106A-5p* directly repressed BTG3 expression through binding the 3'-untranslated region of *BTG3*, the post-translational mechanism underlying the decrease in BTG3 protein levels, such as translational suppression, remains unknown and will be elucidated in future studies.

The MAPK signaling pathway acts downstream of *MIR106A-5p*, which is consistent with the results from our KEGG pathway analysis. Previous studies have confirmed the key negative regulation role of MAPK signaling in autophagy [48]. In the present study, we demonstrated the specificity of the *MIR106A-5p*-BTG3 axis in regulating cellular autophagy and malignant phenotypes by activating MAPK signaling.

Lastly, this study examined how *MIR106A-5p* was upregulated in the context of NPC. According to previous reports, *MIR106A-5p* could be regulated by multiple long noncoding RNAs including *RHOJ/TCL* [49], *HOTAIRM1* [33], *H19* [50], and *OPI5-AS1* [51]. However, there are few reports of the regulation of *MIR106A-5p* by transcription factors. Previous studies have reported that *MIR106A-5p* could be regulated by the transcription factor EGR1 in ovariectomized mice [52]. Interestingly, our study was the first to demonstrate that EGR1 and SOX9 co-bind at the *MIR106A-5p* promoter and regulate the transcription of *MIR106A-5p* in NPC cells. Super-enhancers are clusters of enhancers that are occupied by exceptionally high densities of transcriptional machinery, including transcription factors, to drive robust expression of genes [53]. It is therefore of great interest to further clarify how EGR1 and SOX9 co-activate *MIR106A-5p* expression and whether super-enhancers drive the overexpression of *MIR106A-5p*.

Overall, this study revealed the role of *MIR106A-5p* in autophagy and promotion of the NPC malignant phenotype. Our results suggest that quantification of *MIR106A-5p* is useful for predicting the odds of recurrence and survival prior to treatment. In conclusion, our findings can be used to provide new insights into the clinical application of autophagy-related NPC therapy.

## Materials and methods

### Human NPC specimens

Tissue and serum samples from pathologically confirmed cases of NPC were collected at the Affiliated Hospital of Nantong University following ethics committee approval (IRB number: 2018-L049). All included patients were informed and had not received any cancer therapies prior to biopsy. Tissue microarrays examining *MIR106A-5p*, *BTG3*, and *SOX9* expression were performed by Outdo Biotechnology. Detailed patient clinicopathological features are listed in Table S4. The prognostic significance of *MIR106A-5p*, *BTG3*, and *SOX9* was assessed by Kaplan–Meier analysis. The X-tile Software (version 3.6.1; Rimm Lab; Yale School of Medicine) was used to define *MIR106A-5p*, *BTG3*, and *SOX9* low and high expression before survival analysis.

### Cell culture

The normal nasopharynx epithelial cell line NP69 and the human NPC cell lines 6–10B (low tumorigenesis and low metastasis), 5–8 F (high tumorigenesis and high metastasis), CNE-2 (low differentiation), and CNE-1 (high differentiation) were as gift from the Sun Yat-Sen University and Xiang-Ya School of Medicine, which were cultured in the Otolaryngology Laboratory, Affiliated Hospital of Nantong

University. NPC cells were cultured in RPMI 1640 (Biological Industries Israel Beit-Haemek, 01-100-1ACS) containing 10% FBS (Biological Industries Israel Beit-Haemek, 04-001-1ACS), and NP69 cells were maintained in keratinocyte-SFM (Thermo Fisher Scientific, 17005-042). Cells were grown at 37°C with 5% CO<sub>2</sub>. The CNE2 cell line was recently authenticated using short tandem repeat analysis [54].

### **Transfection and transduction with plasmids, siRNAs, lentiviral vectors, miRNA sponges, inhibitors, and mimics**

All transfection experiments were performed as previously described [54]. Plasmids, siRNAs, lentiviral vectors, miRNA sponges, inhibitors, and mimics, along with their respective controls, were designed and obtained from Shanghai Genechem Co.Ltd. Sequences are shown in Table S5. A tandem monomeric RFP-GFP-tagged MAP1LC3 (Shanghai Genechem Co.Ltd, tFLC3) was used to determine autophagic flux.

### **qRT-PCR**

**RNA isolation and qRT-PCR:** qRT-PCR was performed as described previously [54]. Briefly, total RNA was isolated with Trizol (Thermo Fisher Scientific, 15596018), reverse transcribed to single-strand cDNA, and amplified using primers for *BTG3* and *SOX9*. For qRT-PCR amplification, the reaction was performed in a 20  $\mu$ L reaction volume containing 10  $\mu$ L SYBR Green PCR Master Mix (Roche, 04913914001) using a Real-Time PCR System (Stepone P, Applied Biosystems, Grand Island, NY). Relative mRNA expression levels were normalized to *GAPDH*. The sequences of primers are listed in Table S6.

**miRNA isolation and qRT-PCR:** miRNAs were isolated using Trizol and the miRcute Serum/Plasma miRNA isolation Kit (TIANGEN, DP501). Bulge-loop<sup>TM</sup> miRNA qRT-PCR Prime Sets (one RT primer and a pair of qPCR primers for each set) specific for *MIR106A-5p* and *MIR106B-5p* are designed by Guangzhou Ribobio. cDNA synthesized from miRNAs were amplified with primers for *MIR106A-5p* and *MIR106B-5p*. Serum levels of *MIR106A-5p* were normalized to *cel-MIR39*, whereas tissue and cell levels of *MIR106A-5p* and *MIR106B-5p* were normalized to *RNU6*.

### **Zebrafish tumor model and microinjection**

Zebrafish tumor models were developed as previously described [22]. Animals were housed in the Laboratory Zebrafish Center at Nantong University. For tumor cell inoculation, 300 tumor cells in 5 nL RPMI 1640 medium labeled with 2 g/mL DiI (Beyotime, C1036) were injected into the perivitelline cavity of zebrafish embryos at 48 h post-fertilization using a microinjection system (WPI, Sarasota, Florida, USA).

### **BALB/c nude mice animal models**

To assess the role of *MIR106A-5p* on NPC lung metastasis *in vivo*, CNE-2 cells were transfected with *MIR106A-5p*-

specific sponges or empty vector. After that,  $2 \times 10^6$  luciferase-labeled CNE-2 cells in 100  $\mu$ L RPMI 1640 medium were injected into the tail veins of 7 to 8-week-old male nude mice ( $n = 3$  per group). To confirm the successful injection, the photon flux from the whole body of the mice was measured using the IVIS Lumina Series III (Caliper Life Sciences, Mountain View, CA, USA) weekly. Over the course of 7 weeks, the BLI analysis of each mouse was performed to monitor for lung metastasis.

To identify the function of *MIR106A-5p*-suppressed autophagy in NPC lung metastasis, *MIR106A-5p*-knockdown CNE-2 cells were transfected with or without lentiviral *ATG5* shRNA. A volume of 100  $\mu$ L RPMI 1640 medium containing  $2 \times 10^6$  luciferase-labeled cancer cells were injected into the tail vein of nude mice ( $n = 3$  per group). The lung metastasis was monitored with BLI analysis over the course of 7 weeks.

To corroborate the role of *MIR106A-5p*-*BTG3* axis results in NPC lung metastasis, NPC cells treated with *MIR106A-5p* sponges were transduced with lentiviral *BTG3*-shRNA or empty vector. The resultant cells were injected into the tail veins of nude mice ( $n = 3$  per group) at a volume of  $2 \times 10^6$  cancer cells. Over the course of 7 weeks, BLI was detected.

Animal xenograft tumor model analysis was performed as previously described [54]. In brief, 5-week-old male BALB/c mice were obtained from the Laboratory Animal Center of Nantong University and subcutaneously injected with  $1 \times 10^6$  NPC cells with or without knockdown of *MIR106A-5p*, *ATG5*, or *BTG3*. The mice were monitored daily for changes in tumor size with sliding calipers. All the mice were sacrificed 21 d after inoculation. The primary tumors were removed, fixed in 10% formalin, embedded in paraffin, and subjected to IHC.

### **ISH**

ISH for *MIR106A-5p* was performed using the LNATM microRNA ISH kit (Exiqon, YD00610154-BCG) as previously described [54]. Staining intensity and abundance of positive cells were divided into four grades: 1 (negative), 2 (weakly positive), 3 (moderately positive), and 4 (strongly positive) for staining intensity and 1 (0–25%), 2 (26–50%), 3 (51–75%), and 4 (>75%) for positive cell proportion. The final staining score was defined as the product of the two scores, with scores of 0–8 defined as *MIR106A-5p* low expression and scores of 9–16 defined as *MIR106A-5p* high expression.

### **IF**

IF assays were performed as described previously [55]. Slides were incubated with primary antibodies for MAP1LC3 (Cell Signaling Technology, 14600-1-AP; 1:200) and MKI67 (Proteintech, 27309-1-AP; 1:100) and visualized using Alexa Fluor-conjugated secondary antibodies (Invitrogen, A-11008). Slides were counterstained with Hoechst (Thermo Fisher Scientific, 62249) and imaged using confocal laser scanning microscopy (Leica Microsystems, Wetzlar, Germany, TCS SP-5).

### Transmission electron microscopy

Transmission electron microscopy was performed as described previously [56]. Briefly, 2.5% glutaraldehyde-fixed cells were post-fixed with 1% osmic acid (Sigma-Aldrich, O5500) followed by acetone dehydration. Dehydrated pellets were embedded in araldite CY212 for sectioning, followed by staining with alcoholic uranyl acetate (Polysciences, Inc., 6159-44-0) and alkaline lead citrate (Sigma-Aldrich, 15326). Autophagic vacuoles of the ultrathin sections were examined under a transmission electron microscope (JEOL Ltd, Tokyo, Japan, JEM-1230).

### Spheroid formation and LIVE/DEAD Viability assay

A total of 20,000 CNE-2 cells were plated into Corning 96-well spheroid microplates (Corning, 4515), and spheroids were examined after 7 d. Following this, cells were stained using the LIVE/DEAD® Viability/Cytotoxicity Kit following the manufacturer's protocols (Thermo Fisher Scientific, L3224). Cells were washed with phosphate-buffered saline (PBS; Gibco, 10010023), and 100 µL of a solution comprising 10 mL of PBS with 20 µL of 2 mM EthD-1 (Thermo Fisher Scientific, L3224) and 5 µL of 4 mM calcein AM (Thermo Fisher Scientific, L3224) was added to the microplates. Cells were incubated in this solution for 30 min at room temperature and imaged using fluorescence microscopy (Zeiss, Göttingen, German, Axio Obse).

### ChIP

ChIP was performed with the ChIP Assay Kits (Merck, 17-295) following the manufacturer's protocol. Briefly, cells were cross-linked with 1% formaldehyde and sonicated to generate DNA fragments between 200 and 1000 bp. The precleared supernatant was then incubated with antibodies against EGR1 (Santa Cruz

Biotechnology, sc-101033; 5 µg; polyclonal mouse), SOX9 (Abcam, ab3697; 5 µg; polyclonal rabbit), or an isotype control IgG (Millipore; 345701, 1 µg; mouse IgG). PCR was performed using primers for *MIR106A-5p* promoter-binding sites (EGR1: [forward] 5'-TGGGATCTTCCGCCTCCATTC-3', [reverse] 5'-CCAGGATGAGAAGTTTGTGTCCTCA-3'; SOX9: [forward] 5'-CAGTTGGGAAGTTGATCCAGACAT-3', [reverse] 5'-ACCCCTCCTCCCAGTCCTC-3'). DNA isolated from total nuclear extract was used as the PCR input control, and PCR products were analyzed by gel electrophoresis using a 2% agarose gel.

### Luciferase reporter assay

Assays were performed as described previously [54]. Briefly, wild-type *BTG3* (NM\_001130914.1) 3'-UTR segments were PCR-amplified and inserted into the pGL3-Control vector (Promega, E1741) to generate *BTG3* wild-type plasmids. Mutant 3'-UTR segments of *BTG3* (*BTG3* MUT1) containing mutated sequences at *MIR106A-5p* complementary sites were generated by performing site-directed mutation of the wild-type *BTG3* plasmid.

Primers used in the cloning experiments were as follows:

Human *BTG3*-3'UTR-XhoI-left:

5'-CTCGAGTCTTAAAAAATATATGCACTTTAAAGC  
TT-3'

Human *BTG3*-3'UTR-HindIII-right:

5'-AAGCTTTAAAGTGCATATATTTTTTAAGACTC  
GAG-3'

Human *BTG3*-3'-MUTR-XhoI-left:

5'-CTCGAGTCTTAAAAAATATGTATTCCTACTAAA  
GCTT-3'

Human *BTG3*-3'-MUTR-HindIII-right:

5'-AAGCTTTAGTGAATACATATTTTTTAAGACT  
CGAG-3'

**Table 1.** Antibodies used for western blot and immunohistochemistry.

Antibodies	Manufacturer	Catalog numbers	Dilution (WB)	Dilution (IHC)	Dilution (IF)
ATG5	Cell Signaling Technology	12994	1:1000		
MAP1LC3B-I/II	Cell Signaling Technology	14600-1-AP	1:1000	1:500	1:200
SQSTM1	Cell Signaling Technology	8025	1:1000		
p-AKT	Cell Signaling Technology	4060	1:1000		
t-AKT	Cell Signaling Technology	4691	1:1000		
p-MTOR	Cell Signaling Technology	2983	1:1000		
t-MTOR	Cell Signaling Technology	5536	1:1000		
BTG3	Sangon Biotech	D220325	1:100	1:50	
SOX9	Abcam	ab3697	1:200	1:100	
EGR1	Abcam	ab194357	1:200		
MAPK1/3	Sangon Biotech	D160317	1:500		
p-MAPK1/3	Sangon Biotech	D155116	1:500		
ACTB	Sangon Biotech	D110001	1:600		
MKI67	proteintech	27309-1-AP		1:100	1:100
p-MAP2K1/MEK	Cell Signaling Technology	9154	1:1000		
t-MAP2K1/MEK	Cell Signaling Technology	4694	1:1000		
p-MAPK1/ERK	Cell Signaling Technology	4370	1:2000		
t-MAPK1/ERK	Cell Signaling Technology	4695	1:1000		
Cleaved-CASP3	Cell Signaling Technology	9664		1:5000	



## Western blot and IHC

Western blot and IHC were performed as described previously [55]. Antibodies are listed in Table 1. For western blot analysis, 20 µg of lysate were separated on SDS-PAGE gels and transferred to PVDF membrane (Millipore, ISEQ00010). The membrane was incubated with the indicated primary antibodies. ImageJ software was used for analysis and verification that the band detection was within the linear range.

## Transwell assay

Migration assay was performed using Transwell inserts (Corning, 3422) with a pore size of 8 µm. A total of  $5 \times 10^4$  cells suspended in medium without serum were added in the upper chambers, and medium containing 10% fetal bovine serum was added to the lower chambers. After 16 h of incubation, the cells attached to the upper side were removed, and the cells attached to the underside of the membrane were fixed and stained with crystal violet. Digital images were obtained from the membranes, and five random fields were counted per chamber.

## Statistical analysis

Statistical analysis was performed using GraphPad Prism 6 and SPSS 19.0 software. Results from at least three independent experiments are presented as the mean  $\pm$  S.D. Correlation analysis was performed using Spearman's rank correlation coefficient. Survival analysis was analyzed using Kaplan-Meier survival curves. One-way ANOVA and two-tailed Student's t-tests were used to determine statistical significance. P-values of  $P < 0.05$  were considered statistically significant.

## Disclosure statement

The authors have no conflicts of interest to declare with regard to this manuscript.

## Funding

This work was supported by grants from the National Natural Science Foundation of China (Grant No. 81972554, No. 81672682, No. 81602385), the Clinical Frontier Technology of Jiangsu (Grant No. BE2017680), the CSCO Clinical Oncology Research Foundation of Beijing (Grant No. Y-HS2017-074), the Clinical Medical Center of Nantong (Grant No. HS2016001), the innovative research project for postgraduate students of Jiangsu province (Grant No. SJCX19\_0871, No. SJCX19\_0872, No. SJCX18\_0822).

## Ethical approval

This study received ethics approval from the Affiliated Hospital of Nantong University (IRB number: 2018-L049).

*In vivo* studies were approved by the committee on the Ethics of Animal Experiments of Nantong University (RDD number: 20180227-008). All mouse experiments followed NIH Guidelines and were approved by the Administration Committee of Experimental Animals, Jiangsu Province, China (Approval ID: SYXK (SU) 2007-0021).

## References

- Chua MLK, Wee JTS, Hui EP, et al. Nasopharyngeal carcinoma. *Lancet*. 2016;387(10022):1012–1024.
- Croce CM. Causes and consequences of microRNA dysregulation in cancer. *Nat Rev Genet*. 2009;10(10):704–714.
- Suzuki HI, Katsura A, Matsuyama H, et al. MicroRNA regulons in tumor microenvironment. *Oncogene*. 2015;34(24):3085–3094.
- Volinia S, Calin GA, Liu CG, et al. A microRNA expression signature of human solid tumors defines cancer gene targets. *Proc Natl Acad Sci U S A*. 2006;103(7):2257–2261.
- Li H, Jin X, Chen B, et al. Autophagy-regulating microRNAs: potential targets for improving radiotherapy. *J Cancer Res Clin Oncol*. 2018;144(9):1623–1634.
- Galluzzi L, Pietrocola F, Levine B, et al. Metabolic control of autophagy. *Cell*. 2014;159(6):1263–1276.
- Doherty J, Baehrecke EH. Life, death and autophagy. *Nat Cell Biol*. 2018;20(10):1110–1117.
- Zhan L, Li J, Wei B. Autophagy therapeutics: preclinical basis and initial clinical studies. *Cancer Chemother Pharmacol*. 2018;82(6):923–934.
- Katheder NS, Khezri R, O'Farrell F, et al. Microenvironmental autophagy promotes tumour growth. *Nature*. 2017;541(7637):417–420.
- Liang XH, Jackson S, Seaman M, et al. Induction of autophagy and inhibition of tumorigenesis by beclin 1. *Nature*. 1999;402(6762):672–676.
- Henry WS, Laszewski T, Tsang T, et al. Aspirin suppresses growth in PI3K-Mutant breast cancer by activating AMPK and inhibiting mTORC1 signaling. *Cancer Res*. 2017;77(3):790–801.
- Bae SY, Byun S, Bae SH, et al. TPT1 (tumor protein, translationally-controlled 1) negatively regulates autophagy through the BECN1 interactome and an MTORC1-mediated pathway. *Autophagy*. 2017;13(5):820–833.
- Bishop E, Bradshaw TD. Autophagy modulation: a prudent approach in cancer treatment? *Cancer Chemother Pharmacol*. 2018;82(6):913–922.
- Guo W, Wang H, Yang Y, et al. Down-regulated miR-23a contributes to the metastasis of cutaneous melanoma by promoting autophagy. *Theranostics*. 2017;7(8):2231–2249.
- Huang L, Hu C, Cao H, et al. MicroRNA-29c increases the chemosensitivity of pancreatic cancer cells by inhibiting USP22 mediated autophagy. *Cell Physiol Biochem*. 2018;47(2):747–758.
- Hu JL, He GY, Lan XL, et al. Inhibition of ATG12-mediated autophagy by miR-214 enhances radiosensitivity in colorectal cancer. *Oncogenesis*. 2018;7(2):16.
- Wu H, Liu C, Yang Q, et al. MIR145-3p promotes autophagy and enhances bortezomib sensitivity in multiple myeloma by targeting HDAC4. *Autophagy*. 2019;16(4):683–697.
- Li X, Zhu Y, Zhang H, et al. MicroRNA-106a-5p inhibited c2c12 myogenesis via targeting PIK3R1 and modulating the PI3K/AKT signaling. *Genes (Basel)*. 2018;9:7.
- Yang G, Zhang R, Chen X, et al. MiR-106a inhibits glioma cell growth by targeting E2F1 independent of p53 status. *J Mol Med (Berl)*. 2011;89(10):1037–1050.
- Xia X, Lu H, Li C, et al. miR-106b regulates the proliferation and differentiation of neural stem/progenitor cells through Tp53inp1-Tp53-Cdkn1a axis. *Stem Cell Res Ther*. 2019;10(1):282.
- Lee SL, Rouhi P, Dahl Jensen L, et al. Hypoxia-induced pathological angiogenesis mediates tumor cell dissemination, invasion, and metastasis in a zebrafish tumor model. *Proc Natl Acad Sci U S A*. 2009;106(46):19485–19490.
- Shan Y, You B, Shi S, et al. Hypoxia-induced matrix metalloproteinase-13 expression in exosomes from nasopharyngeal carcinoma enhances metastases. *Cell Death Dis*. 2018;9(3):382.
- Gou WF, Yang XF, Shen DF, et al. The roles of BTG3 expression in gastric cancer: a potential marker for carcinogenesis and a target molecule for gene therapy. *Oncotarget*. 2015;6(23):19841–19867.
- Schmelzle T, Hall MN. TOR, a central controller of cell growth. *Cell*. 2000;103(2):253–262.

- [25] Tan G, Tang X, Tang F. The role of microRNAs in nasopharyngeal carcinoma. *Tumour Biol.* 2015;36(1):69–79.
- [26] Luo B, Kang N, Chen Y, et al. Oncogene miR-106a promotes proliferation and metastasis of prostate cancer cells by directly targeting PTEN in vivo and in vitro. *Minerva Med.* 2018;109(1):24–30.
- [27] Wang Z, Wang B, Shi Y, et al. Oncogenic miR-20a and miR-106a enhance the invasiveness of human glioma stem cells by directly targeting TIMP-2. *Oncogene.* 2015;34(11):1407–1419.
- [28] Mendell JT. miRiad roles for the miR-17-92 cluster in development and disease. *Cell.* 2008;133(2):217–222.
- [29] Chen C, Lu Z, Yang J, et al. MiR-17-5p promotes cancer cell proliferation and tumorigenesis in nasopharyngeal carcinoma by targeting p21. *Cancer Med.* 2016;5(12):3489–3499.
- [30] Hu Z, Zhou S, Luo H, et al. miRNA-17 promotes nasopharyngeal carcinoma radioresistance by targeting PTEN/AKT. *Int J Clin Exp Pathol.* 2019;12(1):229–240.
- [31] Deng P, Wu Y. Knockdown of miR-106a suppresses migration and invasion and enhances radiosensitivity of hepatocellular carcinoma cells by upregulating FBXW7. *Int J Clin Exp Pathol.* 2019;12(4):1184–1193.
- [32] Liu J, Huang Y, Wang H, et al. MiR-106a-5p promotes 5-FU resistance and the metastasis of colorectal cancer by targeting TGFbetaR2. *Int J Clin Exp Pathol.* 2018;11(12):5622–5634.
- [33] Chao H, Zhang M, Hou H, et al. HOTAIRM1 suppresses cell proliferation and invasion in ovarian cancer through facilitating ARHGAP24 expression by sponging miR-106a-5p. *Life Sci.* 2020;243:117296.
- [34] Yang H, Ni HM, Ding WX. The double-edged sword of MTOR in autophagy deficiency induced-liver injury and tumorigenesis. *Autophagy.* 2019;15(9):1671–1673.
- [35] Lin DC, Meng X, Hazawa M, et al. The genomic landscape of nasopharyngeal carcinoma. *Nat Genet.* 2014;46(8):866–871.
- [36] Yang Q, Zhang MX, Zou X, et al. A prognostic bio-model based on SQSTM1 and N-stage identifies nasopharyngeal carcinoma patients at high risk of metastasis for additional induction chemotherapy. *Clin Cancer Res.* 2018;24(3):648–658.
- [37] Zhu JF, Huang W, Yi HM, et al. Annexin A1-suppressed autophagy promotes nasopharyngeal carcinoma cell invasion and metastasis by PI3K/AKT signaling activation. *Cell Death Dis.* 2018;9(12):1154.
- [38] Mo N, Lu YK, Xie WM, et al. Inhibition of autophagy enhances the radiosensitivity of nasopharyngeal carcinoma by reducing Rad51 expression. *Oncol Rep.* 2014;32(5):1905–1912.
- [39] Lin YT, Wang HC, Hsu YC, et al. Capsaicin induces autophagy and apoptosis in human nasopharyngeal carcinoma cells by downregulating the PI3K/AKT/mTOR Pathway. *Int J Mol Sci.* 2017;18:7.
- [40] Ai J, Li W, Zeng R, et al. Blockage of SSRP1/Ets-1/Pim-3 signaling enhances chemosensitivity of nasopharyngeal carcinoma to docetaxel in vitro. *Biomed Pharmacother.* 2016;83:1022–1031.
- [41] Lin YT, Wang HC, Chuang HC, et al. Pre-treatment with angiotensin-(1-7) inhibits tumor growth via autophagy by downregulating PI3K/Akt/mTOR signaling in human nasopharyngeal carcinoma xenografts. *J Mol Med (Berl).* 2018;96(12):1407–1418.
- [42] Cheng JZ, Chen JJ, Wang ZG, et al. MicroRNA-185 inhibits cell proliferation while promoting apoptosis and autophagy through negative regulation of TGF-beta1/mTOR axis and HOXC6 in nasopharyngeal carcinoma. *Cancer Biomark.* 2018;23(1):107–123.
- [43] Hai B, Ma Y, Pan X, et al. Melatonin benefits to the growth of human annulus fibrosus cells through inhibiting miR-106a-5p/ATG7 signaling pathway. *Clin Interv Aging.* 2019;14:621–630.
- [44] Chen K, Pan G. Dysregulation of microRNA-106a-5p-RUNX1 axis associates with clinical progression and prognosis of osteosarcoma patients. *Pathol Res Pract.* 2019;215(12):152686.
- [45] Hao H, Xia G, Wang C, et al. miR-106a suppresses tumor cells death in colorectal cancer through targeting ATG7. *Med Mol Morphol.* 2017;50(2):76–85.
- [46] Wang X, Blagden C, Fan J, et al. Runx1 prevents wasting, myofibrillar disorganization, and autophagy of skeletal muscle. *Genes Dev.* 2005;19(14):1715–1722.
- [47] Chen X, Chen G, Cao X, et al. Downregulation of BTG3 in non-small cell lung cancer. *Biochem Biophys Res Commun.* 2013;437(1):173–178.
- [48] Levy JMM, Towers CG, Thorburn A. Targeting autophagy in cancer. *Nat Rev Cancer.* 2017;17(9):528–542.
- [49] Luo LH, Jin M, Wang LQ, et al. Long noncoding RNA TCL6 binds to miR-106a-5p to regulate hepatocellular carcinoma cells through PI3K/AKT signaling pathway. *J Cell Physiol.* 2020;235:6154–6166.
- [50] Zhang X, Liu X, Ni X, et al. Long non-coding RNA H19 modulates proliferation and apoptosis in osteoarthritis via regulating miR-106a-5p. *J Biosci.* 2019;44:6.
- [51] Wang LW, Li XB, Liu Z, et al. Long non-coding RNA OIP5-AS1 promotes proliferation of gastric cancer cells by targeting miR-641. *Eur Rev Med Pharmacol Sci.* 2019;23(24):10776–10784.
- [52] Cong J, Wang C, Pu D, et al. Expression of early growth response 1 affects miR-106a/signal transducer and activator of transcription 3 regulating cognitive impairment in ovariectomized mice. *Menopause.* 2014;21(10):1143–1150.
- [53] Jiang Y, Jiang YY, Xie JJ, et al. Co-activation of super-enhancer-driven CCAT1 by TP63 and SOX2 promotes squamous cancer progression. *Nat Commun.* 2018;9(1):3619.
- [54] Bao L, You B, Shi S, et al. Metastasis-associated miR-23a from nasopharyngeal carcinoma-derived exosomes mediates angiogenesis by repressing a novel target gene TSGA10. *Oncogene.* 2018;37(21):2873–2889.
- [55] You B, Shan Y, Shi S, et al. Effects of ADAM10 upregulation on progression, migration, and prognosis of nasopharyngeal carcinoma. *Cancer Sci.* 2015;106(11):1506–1514.
- [56] Sun Y, Huang YH, Huang FY, et al. 3'-epi-12beta-hydroxyfroside, a new cardenolide, induces cytoprotective autophagy via blocking the Hsp90/Akt/mTOR axis in lung cancer cells. *Theranostics.* 2018;8(7):2044–2060.